Dynamic stiffness of suction caissons

Ibsen, Lars Bo; Liingaard, Morten; Andersen, Lars Vabbersgaard

Publication date:
2006

Document Version
Publisher's PDF, also known as Version of record

Dynamic stiffness of suction caissons - torsion, sliding and rocking

Lars Bo Ibsen
Morten Liingaard
Lars Andersen

ISSN 1901-726X
DCE Technical Report No. 8

AALBORG UNIVERSITY
Department of Civil Engineering

Aalborg University
Department of Civil Engineering
Division of Water and Soil

DCE Technical Report No. 8

Dynamic stiffness of suction caissons - torsion, sliding and rocking

by

Lars Bo Ibsen
Morten Liingaard
Lars Andersen

December 2006

Scientific Publications at the Department of Civil Engineering

Technical Reports are published for timely dissemination of research results and scientific work carried out at the Department of Civil Engineering (DCE) at Aalborg University. This medium allows publication of more detailed explanations and results than typically allowed in scientific journals.

Technical Memoranda are produced to enable the preliminary dissemination of scientific work by the personnel of the DCE where such release is deemed to be appropriate. Documents of this kind may be incomplete or temporary versions of papers—or part of continuing work. This should be kept in mind when references are given to publications of this kind.

Contract Reports are produced to report scientific work carried out under contract. Publications of this kind contain confidential matter and are reserved for the sponsors and the DCE. Therefore, Contract Reports are generally not available for public circulation.

Lecture Notes contain material produced by the lecturers at the DCE for educational purposes. This may be scientific notes, lecture books, example problems or manuals for laboratory work, or computer programs developed at the DCE.

Theses are monograms or collections of papers published to report the scientific work carried out at the DCE to obtain a degree as either PhD or Doctor of Technology. The thesis is publicly available after the defence of the degree.

Latest News is published to enable rapid communication of information about scientific work carried out at the DCE. This includes the status of research projects, developments in the laboratories, information about collaborative work and recent research results.

Published 2006 by
Aalborg University
Department of Civil Engineering
Sohngaardsholmsvej 57,
DK-9000 Aalborg, Denmark

Printed in Denmark at Aalborg University

ISSN 1901-726X
DCE Technical Report No. 8

Preface

The technical report "Dynamic stiffness of suction caissons—torsion, sliding and rocking" is divided into six numbered sections, and a list of references is situated after the last section. Tables, equations and figures are indicated with consecutive numbers. Cited references are marked as e.g. Novak and Sachs (1973), with author specification and year of publication in the text.

The work within this report has only been possible with the financial support from the Energy Research Programme (ERP)[1] administered by the Danish Energy Authority. The project is associated with the ERP programme "Soil–Structure interaction of Foundations for Offshore Wind Turbines". The funding is sincerely acknowledged.

Aalborg, December 13, 2006 Lars Bo Ibsen, Morten Liingaard & Lars Andersen

[1] In danish: "Energiforskningsprogrammet (EFP)"

Contents

1 Dynamic stiffness of suction caissons—torsion, sliding and rocking **1**
1.1 Introduction . . . 1
1.2 Previous work . . . 2
1.3 Static and dynamic stiffness formulation . . . 2
1.4 Dynamic stiffness for torsional vibrations . . . 4
1.4.1 Boundary Element/Finite Element model . . . 4
1.4.2 Static stiffness . . . 5
1.4.3 Dynamic stiffness . . . 5
1.4.4 High-frequency limit . . . 7
1.5 Dynamic stiffness for coupled sliding–rocking vibrations . . . 9
1.5.1 Boundary Element/Finite Element model . . . 9
1.5.2 Static stiffness . . . 9
1.5.3 Dynamic stiffness—variation of Poisson's ratio . . . 10
1.5.4 Dynamic stiffness—variation of skirt length . . . 14
1.5.5 High-frequency limit . . . 17
1.6 Conclusion . . . 17
1.6.1 Torsional vibrations . . . 17
1.6.2 Coupled sliding–rocking vibrations . . . 18

References **19**

List of Figures

1.1 Degrees of freedom for a rigid surface footing: (a) displacements and rotations, and (b) forces and moments. 3
1.2 Geometry (a) and BE/FE model (b) of the suction caisson. 4
1.3 Infinite hollow cylinder (a) and two-dimensional BE/FE model (b) of the cylinder where Ω_i and Ω_o are the inner and outer boundary element domains, respectively. 6
1.4 Torsional impedance: variation of skirt length. $G_s = 1.0$ MPa, $\nu_s = 1/3$ and $\eta_s = 5\%$. 7
1.5 Sliding impedance: variation of Poisson's ratio. $G_s = 1.0$ MPa and $\eta_s = 5\%$. 11
1.6 Rocking impedance: variation of Poisson's ratio. $G_s = 1.0$ MPa and $\eta_s = 5\%$. 12
1.7 Coupling impedance: variation of Poisson's ratio. $G_s = 1.0$ MPa and $\eta_s = 5\%$. 13
1.8 Sliding impedance: variation of skirt length. $G_s = 1.0$ MPa, $\nu_s = 1/3$ and $\eta_s = 5\%$. 14
1.9 Rocking impedance: variation of skirt length. $G_s = 1.0$ MPa, $\nu_s = 1/3$ and $\eta_s = 5\%$. 15
1.10 Coupling impedance: variation of skirt length. $G_s = 1.0$ MPa, $\nu_s = 1/3$ and $\eta_s = 5\%$. 16

List of Tables

1.1 Static torsional stiffness for different skirt lengths 5
1.2 Coupled static stiffness. 10

Chapter 1
Dynamic stiffness of suction caissons—torsion, sliding and rocking

This report concerns the dynamic soil–structure interaction of steel suction caissons applied as foundations for offshore wind turbines. An emphasis is put on torsional vibrations and coupled sliding/rocking motion, and the influence of the foundation geometry and the properties of the surrounding soil is examined. The soil is simplified as a homogenous linear viscoelastic material and the dynamic stiffness of the suction caisson is expressed in terms of dimensionless frequency-dependent coefficients corresponding to the different degrees of freedom. The dynamic stiffness coefficients for the skirted foundation are evaluated by means of a three-dimensional coupled boundary element/finite element model. Comparisons with known analytical and numerical solutions indicate that the static and dynamic behaviour of the foundation are predicted accurately with the applied model. The analysis has been carried out for different combinations of the skirt length and the Poisson's ratio of the subsoil. Finally, the high-frequency impedance has been determined for future use in lumped-parameter models of wind turbine foundations in aero-elastic codes.

1.1 Introduction

Modern offshore wind turbines are flexible structures with resonance frequencies as low as 0.15 Hz. Typically, this is close to the excitation frequencies related to waves and turbine blades passing the tower. Thus a small change in the structural stiffness may result in great changes in the response, for which reason a reliable computation of the structural stiffness is required. This necessitates an accurate prediction of the soil–structure interaction which is highly dependent on the properties of the soil as well as the geometry of the foundation. A novel foundation method for offshore wind turbines is the monopod suction caisson (Houlsby et al. 2005). For this particular kind of foundation, the vertical component of the dynamic stiffness has been discussed in Ibsen and Liingaard (2006a). By contrast, the focus of the present analysis is the impedance related to torsional vibrations and coupled sliding/rocking motion. The previous work related to the analysis of torsional vibrations and coupled sliding/rocking is briefly presented in Section 1.2. Subsequently, a definition of the static and dynamic stiffnesses for the

suction caisson is provided in Section 1.3. The analysis of the torsional dynamic stiffness of the suction caisson is presented in Section 1.4 and the results obtained by analysing the coupled sliding and rocking motion are given in Section 1.5. The main conclusions of the report are given in Section 1.6. In this report the impedance is equal to the dynamic stiffness of the foundation, i.e. the impedance contains both a real and an imaginary part. The frequency dependent dynamic stiffness of the suction caisson is evaluated in the frequency domain by means of the three-dimensional coupled Boundary Element/Finite Element Method program BEASTS by Andersen and Jones (2001). The basic concepts of the method and the preliminary benchmark tests to ensure that the applied numerical model is able to capture the dynamic behaviour of the suction caisson are described in Ibsen and Liingaard (2006a).

1.2 Previous work

Luco and Westmann (1971) investigated the torsional vibrations of a circular massless footing resting on a homogeneous elastic half-space. They solved the system as a mixed boundary value problems with prescribed conditions under the foundation and zero traction at the remaining free surface. The integral equations of the mixed boundary value problems were evaluated and tabulated for a number of excitation frequencies. The effects of material damping on torsionally excited footings were reported by Veletsos and Damodaran Nair (1974), while Wong and Luco (1985) presented tables of horizontal, coupling, rocking, vertical and torsional impedance functions for rigid massless square foundations resting on layered viscoelastic soil. The impedance functions for rigid square foundations embedded in a uniform elastic half-space have been evaluated by means of a hybrid approach by Mita and Luco (1989). Emperador and Domínguez (1989) applied the boundary element method for analysis of the dynamic response of axisymmetric embedded foundations. Approximate closed-form solutions for the torsional impedance of circular embedded foundations have been reported by Novak and Sachs (1973) and Avilés and Pérez-Rocha (1996). The coupled sliding/rocking vibrations of surface footings have been reported by e.g. Veletsos and Wei (1971). This work will be used as the reference solution for the subsequent analyses of the coupled sliding/rocking vibrations of the suction caissons. Bu and Lin (1999) have summarized the work with respect to analyses of coupled sliding/rocking vibrations of foundations and further references will not be repeated here.

1.3 Static and dynamic stiffness formulation

A massless rigid foundation has six degrees of freedom: one vertical, two horizontal (sliding), two rocking and one torsional. The six degrees of freedom and the corresponding forces and moments are shown in Figure 1.1, and in the general case all components of displacement may be coupled. However, in the particular case of axisymmetric foundations there is only a coupling between the horizontal sliding and rocking motion. Thus, the vertical and torsional motion are completely decoupled from each other and from the remaining degrees of freedom. Furthermore, for a circular footing with the radius R it is advantageous to represent the relationship between displacements/rotations and

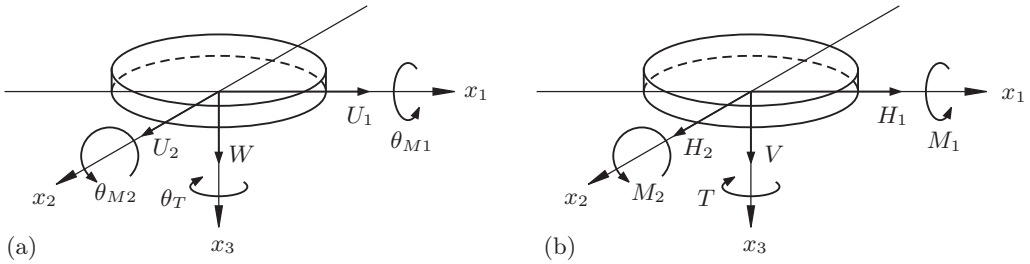

Figure 1.1: Degrees of freedom for a rigid surface footing: (a) displacements and rotations, and (b) forces and moments.

forces/moments in a non-dimensional form. For harmonic excitation with the cyclic frequency ω, the component form can be written as

$$\begin{bmatrix} V/G_sR^2 \\ H_1/G_sR^2 \\ H_2/G_sR^2 \\ T/G_sR^3 \\ M_1/G_sR^3 \\ M_2/G_sR^3 \end{bmatrix} = \begin{bmatrix} S_{VV} & 0 & 0 & 0 & 0 & 0 \\ 0 & S_{HH} & 0 & 0 & 0 & -S_{HM} \\ 0 & 0 & S_{HH} & 0 & S_{HM} & 0 \\ 0 & 0 & 0 & S_{TT} & 0 & 0 \\ 0 & 0 & S_{MH} & 0 & S_{MM} & 0 \\ 0 & -S_{MH} & 0 & 0 & 0 & S_{MM} \end{bmatrix} \begin{bmatrix} W/R \\ U_1/R \\ U_2/R \\ \theta_T \\ \theta_{M1} \\ \theta_{M2} \end{bmatrix}. \quad (1.1)$$

Here G_s is the shear modulus of the soil which is complex if material damping is introduced (see Ibsen and Liingaard (2006a) for details). The coupling terms, S_{HM} and S_{MH}, are assumed to be equal. This assumption is discussed in Subsection 1.5.2. The normalized dynamic stiffness depends on the cyclic frequency, ω, and Poisson's ratio of the soil, ν_s. A formulation that is independent of the mass density of the soil, ρ_s, may be obtained by the introduction of the dimensionless frequency $a_0 = \omega R/c_S$, where $c_S = \sqrt{G_s/\rho_s}$ denotes the shear wave velocity of the soil. The normalized components of the dynamic stiffness matrix given in Equation (1.1) can then be written as

$$S_{ij}(a_0) = K_{ij}^0 \left[k_{ij}(a_0) + \mathrm{i}a_0 c_{ij}(a_0)\right], \qquad (i,j = H,M,T,V), \quad (1.2)$$

where K_{ij}^0 are the corresponding components of the static stiffness matrix and $\mathrm{i} = \sqrt{-1}$ is the imaginary unit. The dimensionless dynamic stiffness and damping coefficients, k_{ij} and c_{ij}, are both real. Both geometrical damping, i.e. the radiation of waves into the subsoil, and possibly also material dissipation contribute to c_{ij}. The stiffness representation provided in terms of real and imaginary parts tends to be inconclusive in some situations. Instead it is convenient to examine the magnitude $|S_{ij}|$ and phase angle ϕ_{ij} of Equation (1.2). These are defined as

$$|S_{ij}| = |K_{ij}^0|\sqrt{(k_{ij})^2 + (a_0 c_{ij})^2}, \qquad \phi_{ij} = \arctan\left(\frac{a_0 c_{ij}}{k_{ij}}\right). \quad (1.3)$$

This representation of the dynamic stiffness will be applied throughout the report.

1.4 Dynamic stiffness for torsional vibrations

In this section the torsional dynamic stiffness is investigated. The Poisson's ratio has no impact on the torsional stiffness, since torsional vibrations of the suction caisson only produce shear waves. Hence, the analysis only concerns the variation of the normalized torsional stiffness due to a change in the skirt length H. The geometry is sketched in Figure 1.2a. This Section consists of four parts. Firstly, the Boundary Element/Finite Element (BE/FE) model applied in the analysis is described. Secondly, the static torsional stiffness obtained by the BE/FE model is presented and compared with results from a static finite element analysis in ABAQUS (Abaqus 2003). Thirdly, the dynamic stiffness for torsional vibrations is examined, and the last subsection presents the asymptotic impedance behaviour in the high frequency range.

1.4.1 Boundary Element/Finite Element model

The BE/FE model of the suction caisson is divided into four sections: a finite element section that forms the top of the foundation (the lid), a finite element section of the skirt, a boundary element domain inside the skirt and, finally, a boundary element domain outside the skirt that also forms the free ground surface. Whereas the lid is massless, the skirt has a mass density corresponding to that of the soil. This produces a model which is directly comparable to a massless surface footing. The skirt of the suction caisson is considered flexible, and the lid is assumed to be rigid. The lid is modelled as a solid finite element section with a thickness of one meter. The elements utilized in the present study are 9-noded quadrilateral boundary elements and 26-noded isoparametric finite elements—both with quadratic spatial interpolation. The model of the suction caisson and the subsoil contains approx. 100 finite elements and 350 boundary elements. The mesh of the free surface is truncated at a distance of 30 m ($\sim 6R$) from the centre of the foundation (see Ibsen and Liingaard (2006a)). The connection between the soil and the foundation corresponds to the condition of 'rough' contact since the foundation and the

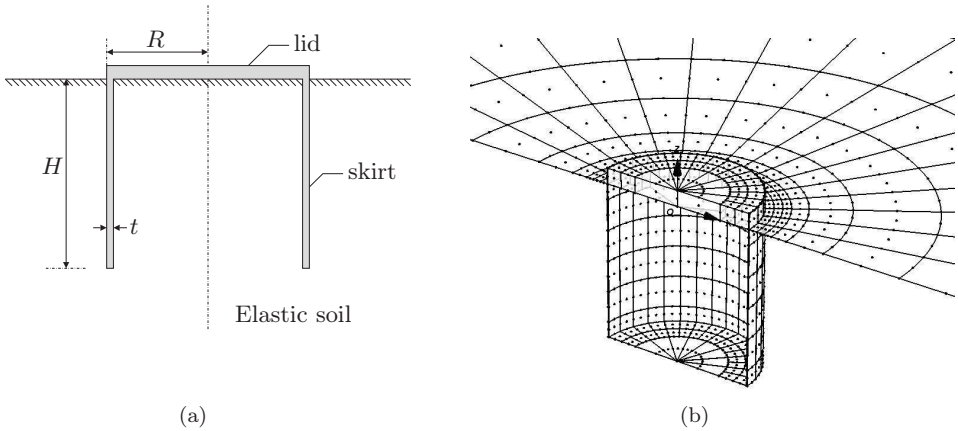

Figure 1.2: Geometry (a) and BE/FE model (b) of the suction caisson.

Table 1.1: Static torsional stiffness for different skirt lengths

H/D	K^0_{TT} FE	K^0_{TT} BE/FE	Deviation
1/4	12.94	13.15	−1.63 %
1	32.36	32.43	−0.23 %
2	56.88	53.90	+5.52 %

surrounding soil have common degrees of freedom. The model is illustrated in Figure 1.2b. Due to geometrical symmetry, only half the foundation is included in the model. In the case of torsion, antisymmetric load and response are assumed. The BE/FE analysis has been carried out for 40 equally spaced excitation frequencies in the range $a_0 \in]0;10]$. For each frequency a pair of opposing horizontal forces are applied at the bottom of the lid in order to create a torque. The resulting torsional response is computed, and the complex dynamic stiffness is then determined as the ratio between the applied moment and the resulting amplitude of the rotation. Note that load control has been used to generate the stiffness values. Displacement control would be more appropriate, but this feature is currently not available in the BE/FE software.

1.4.2 Static stiffness

The static torsional stiffness K^0_{TT} has been computed for three different ratios between the foundation diameter, $D = 2R$, and the skirt length, H. In all cases, the soil properties are $G_s = 1$ MPa and $\nu_s = 1/3$. The foundation material (steel) has the Young's modulus $E_f = 210$ GPa and the Poisson's ratio $\nu_f = 0.25$. The foundation radius is $R = 5$ m and the skirt thickness is $t = 50$ mm. The material properties of the soil and the foundation are identified by the subscripts s and f, respectively. The results obtained with the BE/FE program BEASTS are listed in Table 1.1 for $H/D = 1/4$, 1 and 2. A comparison is made with the finite element solution provided by a three-dimensional ABAQUS model. As indicated by Table 1.1, the two numerical models provide similar results, indicating that both the ABAQUS and BEASTS models are nearly converged. The deviation is properly due to the fact that better convergence has been obtained by the FE solution.

1.4.3 Dynamic stiffness

The normalized torsional dynamic stiffness, $|S_{TT}|/K^0_{TT}$ is analysed for the three normalized skirt lengths, $H/D = 1/4$, 1 and 2, and in the normalized frequency range $a_0 \in]0;10]$. A comparison is made with two reference solutions. Firstly, the normalized torsional dynamic stiffness has been found for a surface footing. This result has been obtained by means of a three-dimensional BE/FE model with no skirt, i.e. with $H = 0$. Secondly, the dynamic stiffness per unit length of an infinite hollow cylinder subjected to dynamic excitation is evaluated by means of the two-dimensional coupled BE/FE program TEA by Jones, Thompson, and Petyt (1999). The hollow cylinder is modelled with 64 quadrilateral finite elements employing quadratic interpolation. The interior and ex-

terior soil domains are modelled with 64 boundary elements each. The model is sketched in Figure 1.3, and plane strain is assumed. In all the analyses, the soil has the shear modulus $G_s = 1$ MPa, the Poisson's ratio $\nu_s = 1/3$, the mass density $\rho_s = 1000$ kg/m^3 and the loss factor $\eta_s = 5\%$. Hysteretic material damping in the soil is assumed, i.e. the loss factor is assumed to be constant for all frequencies. The foundation has the Young's modulus $E_f = 210$ GPa, the Poisson's ratio $\nu_f = 0.25$, the loss factor $\eta_f = 2\%$ and the skirt thickness $t = 50$ mm. In order to model a massless foundation, the mass density is $\rho_f = 0$ for the lid of the caisson and $\rho_f = \rho_s$ for the skirt. As indicated by Figure 1.4, the normalized magnitudes of the torsional impedance are similar for the surface footing, the caissons and the infinite cylinder in the frequency interval $a_0 \in [0;2]$. Note that the actual magnitude of the impedance for each skirt length is scaled by the static values given in Table 1.1. For $a_0 > 2$ the impedance of all the skirted foundations are greater than the impedance of the surface footing. The dynamic stiffness of the caisson with a relatively small embedment depth ($H/D = 1/4$) varies smoothly with the frequency. However, the normalized magnitudes for $H/D = 1$ and 2 are characterized by distinct peaks close to $a_0 = 4$, 7 and 10. The peaks become more pronounced when the skirt length is increased, and the behaviour corresponds well to that of the infinite cylinder. Between the peaks, the normalized torsional impedances for all skirt lengths are nearly identical in magnitude. This is even the case for the infinite cylinder. However, K^0_{TT} (and therefore also $|S_{TT}|$) is increased significantly with an increase in the skirt length, cf. Table 1.1. Further, the local peaks in the normalized magnitude are associated with a significant change in the phase angle, ϕ_{TT}. The fact that the oscillations are repeated for equal distances in frequency implies that the frequencies at the local peaks correspond to anti-resonance modes of the soil inside the suction caisson. This behaviour is similar

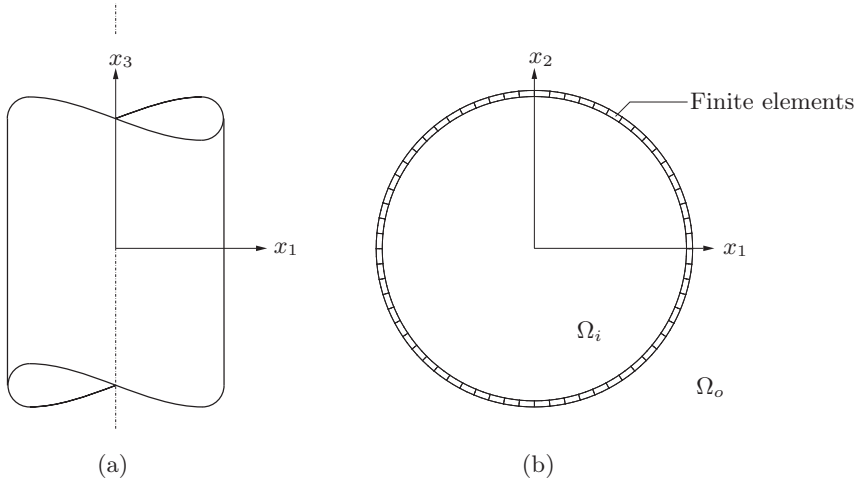

Figure 1.3: Infinite hollow cylinder (a) and two-dimensional BE/FE model (b) of the cylinder where Ω_i and Ω_o are the inner and outer boundary element domains, respectively.

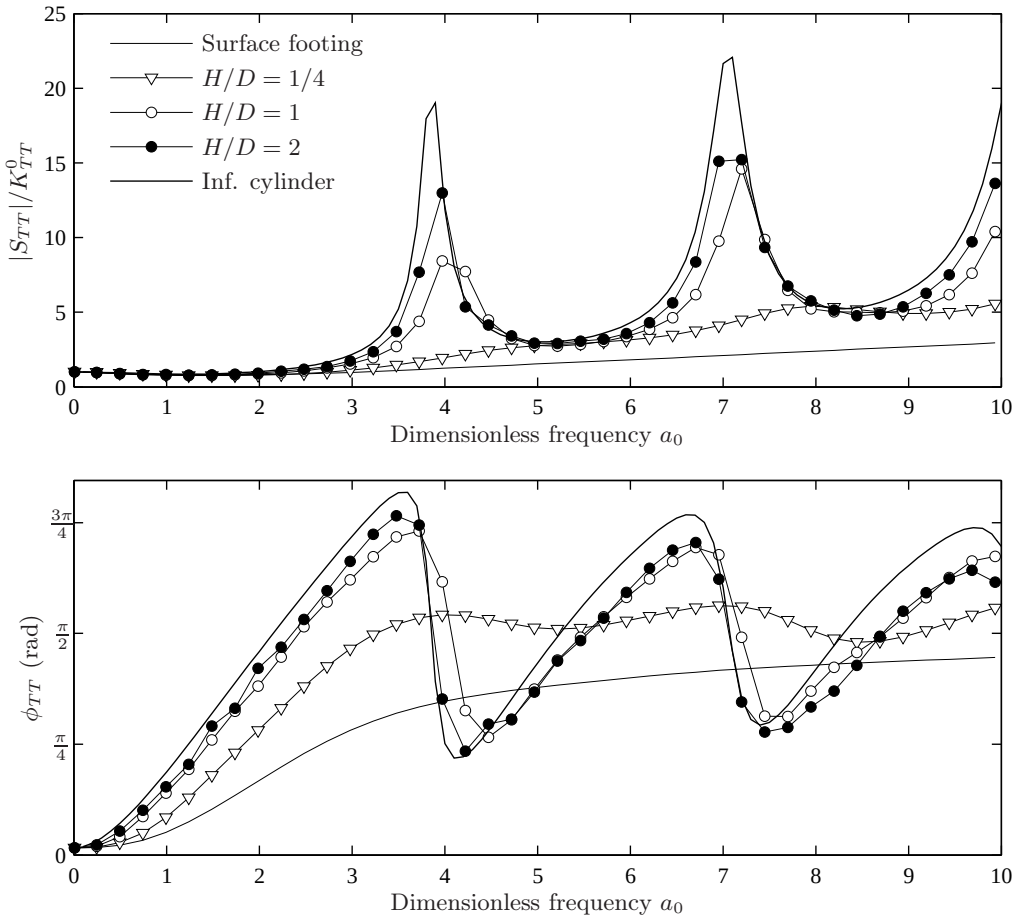

Figure 1.4: Torsional impedance: variation of skirt length. $G_s = 1.0$ MPa, $\nu_s = 1/3$ and $\eta_s = 5\%$.

to the observed behaviour for vertical vibrations as presented in Ibsen and Liingaard (2006a).

1.4.4 High-frequency limit

The limiting damping parameter C^{∞}_{TT} of the suction caisson consists of two contributions: one from the vibration of the lid and one originating from the vibration of the skirt, see Ibsen and Liingaard (2006a). C^{∞}_{TT} of the suction caisson is given by

$$C^{\infty}_{TT} = \rho_s c_S J_{lid} + (2\rho_s c_S A_{skirt})\, R^2, \tag{1.4}$$

where J_{lid} is the polar moment of inertia of the lid about the axis of rotation, and A_{skirt} is the surface area of skirt. Note that S-waves are generated both inside and outside the

skirt, hence the factor '2' in the latter contribution in Equation (1.4). The radius R is the distance from skirt to the axis of rotation.

1.5 Dynamic stiffness for coupled sliding–rocking vibrations

In this section the coupled sliding–rocking vibrations are investigated for several different combinations of the mechanical properties of the soil–foundation system. The first case concerns the effects of Poisson's ratio on the stiffness. The second analysis investigates the variation of the stiffness due to a change in the skirt length. Finally, the limiting damping parameters for vibration in the high-frequency range are given.

1.5.1 Boundary Element/Finite Element model

The geometry and the discretization in the BE/FE models employed for the present analyses are as described in the previous section. However, the load is applied differently. For a given excitation frequency, two analyses are performed: one analysis with horizontal loading at the base of the lid of the caisson, and one analysis with a set of opposing vertical forces that are applied at each side of the foundation in order to create a rocking moment. The first analysis provides a relation between the horizontal force and the resulting displacements and rotations. The second analysis relates the applied moment to the resulting displacements and rotations. The system can be written as a subset of Equation 1.1, given as

$$\begin{bmatrix} H_1/G_sR^2 \\ M_2/G_sR^3 \end{bmatrix} = \begin{bmatrix} S_{HH} & -S_{HM} \\ -S_{MH} & S_{MM} \end{bmatrix} \begin{bmatrix} U_1/R \\ \theta_{M2} \end{bmatrix}. \tag{1.5}$$

The two equations are then solved simultaneously, in order obtain the complex horizontal sliding impedance, S_{HH}, the rocking moment impedance, S_{MM}, and the coupling impedances, S_{HM} and S_{MH}. As already mentioned and further discussed below, $S_{HM} = S_{MH}$ within the precision of the model.

1.5.2 Static stiffness

The static stiffness coefficients of the coupled system have been determined by the BE/FE models for $a_0 = 0.01$, and then compared with the results of static finite element analyses in ABAQUS. The non-dimensional values of K^0_{HH}, K^0_{MM}, K^0_{HM} and K^0_{MH} are given for two different cases:

Different skirt lengths: – The static stiffness components are given for various ratios between the foundation diameter D and the length of the skirt H in Table 1.2. The soil properties are $G_s = 1$ MPa and $\nu_s = 1/3$.

Different Poisson's ratios: – The variation of static stiffness with respect to Poisson's ratio is shown in Table 1.2. $H/D = 1$ and $G_s = 1$ MPa.

Note that the values in parentheses in Table 1.2 are obtained by the static finite element analyses in ABAQUS. The data are shown for fixed material properties of the foundation ($E_f = 210$ GPa, $\nu_f = 0.25$). The foundation radius is $R = 5$ m and the skirt thickness is $t = 50$ mm. In addition to the analyses listed above, it may be relevant to check the influence of the skirt flexibility. However, a preliminary study indicates that changes

Table 1.2: Coupled static stiffness.

		K^0_{HH}		K^0_{MM}		K^0_{HM}		K^0_{MH}	
$H/D =$	1/4	8.00	(7.47)	8.51	(8.41)	-3.13	(-2.68)	-2.78	(-2.68)
	1	13.92	(12.98)	52.91	(49.73)	-18.28	(-16.11)	-17.20	(-16.12)
	2	18.61	(18.47)	198.87	(193.41)	-44.80	(-43.02)	-43.54	(-43.12)
$\nu_s =$	0.1	12.49	(11.62)	49.75	(46.91)	-17.11	(-15.19)	-16.09	(-15.21)
	0.2	13.01	(12.14)	50.83	(47.92)	-17.50	(-15.53)	-16.47	(-15.55)
	0.333	13.92	(12.98)	52.91	(49.73)	-18.28	(-16.11)	-17.20	(-16.12)
	0.4	14.54	(13.53)	54.42	(51.02)	-18.86	(-16.54)	-17.75	(-16.53)
	0.495	15.74	(14.51)	57.79	(53.98)	-20.19	(-17.42)	-18.95	(-17.39)

in E_f and t within the range that is relevant for suction caissons have little impact on the overall performance of the foundation compared with the skirt length and the Poisson's ratio of the ground. Therefore, this study will not be included in the present analysis. The largest deviation between the results from the BE/FE model and the ABAQUS models in Table 1.2 are: 7.4%, 7.2% and 16.8% for the sliding, rocking and coupling term, respectively. Furthermore, the assumption of $K^0_{HM} = K^0_{MH}$ holds true. The maximum deviation between K^0_{HM} and K^0_{MH} is 11% in the BE/FE model and only 3.3% for the ABAQUS model. In general there is a good agreement between the values of the impedance components computed by the FE and the BE/FE models. As expected, all the stiffness components increase with the skirt length, cf. Table 1.2. The magnitude of the sliding, rocking and coupling terms increase slightly with Poisson's ratio, ν_s. This is due to the fact that an increase in ν_s for a fixed value of G_s implies an increase in the Young's modulus, $E_s = 2G_s(1 + \nu_s)$.

1.5.3 Dynamic stiffness—variation of Poisson's ratio

The dynamic stiffness for different Poisson's ratios is presented in this section. The skirt length is fixed ($H/D = 1$), and the model properties are: $G_s = 1.0$ MPa, $\rho_s = 1000$ kg/m^3, $\eta_s = 5\%$, $E_f = 210$ GPa, $\nu_f = 0.25$, $\eta_f = 2\%$ and $t = 50$ mm. In order to model a massless foundation $\rho_f = 0$ for the lid of the caisson and $\rho_f = \rho_s$ for the skirt. In Figures 1.5–1.7, the results are shown for five different values of Poisson's ratio and for the frequency range $a_0 \in]0;6]$. Note that the range in Poisson's ratio is thought to cover fully drained ($\nu_s = 0.1 - 0.2$) to undrained ($\nu_s = 0.495$) conditions. The analytical solution for a surface footing proposed by Veletsos and Wei (1971) is included as reference. Two numerical models of a massless surface footing are included for comparison with the analytical solution. The sliding and rocking impedance of the surface footing have been determined by a BE/FE model. In the case of the coupling between horizontal sliding and rocking, numerical experiments indicate that convergence of the impedance cannot be established with a reasonably low number of degrees of freedom in the BE/FE model. In particular it has been found that both the magnitude and the phase of the impedance is strongly dependent on the distance from the footing to the truncation edge of the free ground surface. Adaptive meshing could possibly improve the accuracy versus the

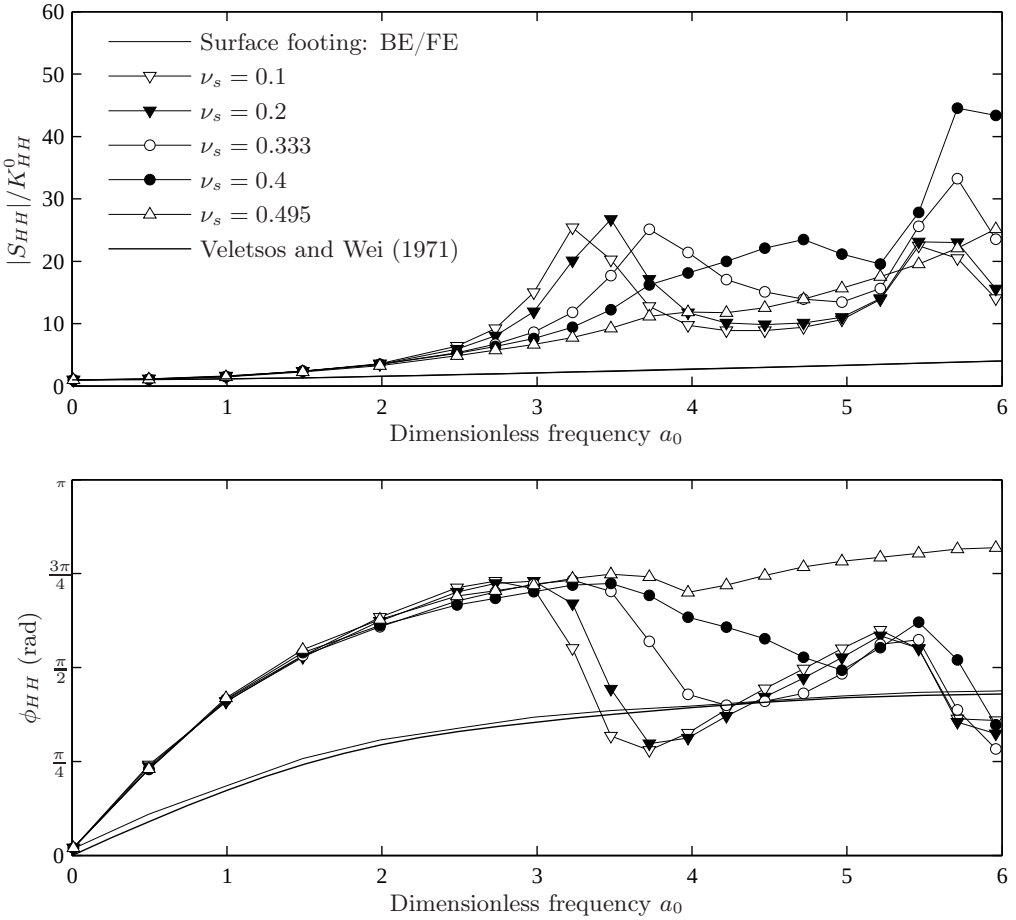

Figure 1.5: Sliding impedance: variation of Poisson's ratio. $G_s = 1.0$ MPa and $\eta_s = 5\%$.

number of degrees of freedom, but this facility is currently not available in the BE/FE software. Therefore, instead of the coupled BE/FE model based on the Green's function for the full-space, an alternative method proposed by Andersen and Clausen (2005) has been applied. Here the solution is established in the wavenumber domain, and the fundamental solution for a half-space is employed. Moreover, the impedance is computed directly by integration of the interaction forces between the footing and the subsoil. This is in contrast to the BE/FE approach, in which the impedance is found by inversion of the dynamic flexibility matrix. The latter approach may involve great inaccuracies with respect to the coupling term since $|S_{HM}|$ is much smaller than $|S_{HH}|$ and $|S_{MM}|$, in particular in the high-frequency range.

The sliding and rocking impedances are clearly dependent on Poisson's ratio. The frequency at the first local extremum in the magnitude of the impedance in Figures 1.5 and 1.6 changes significantly with Poisson's ratio. The first peak for $\nu_s = 0.1$ occurs at

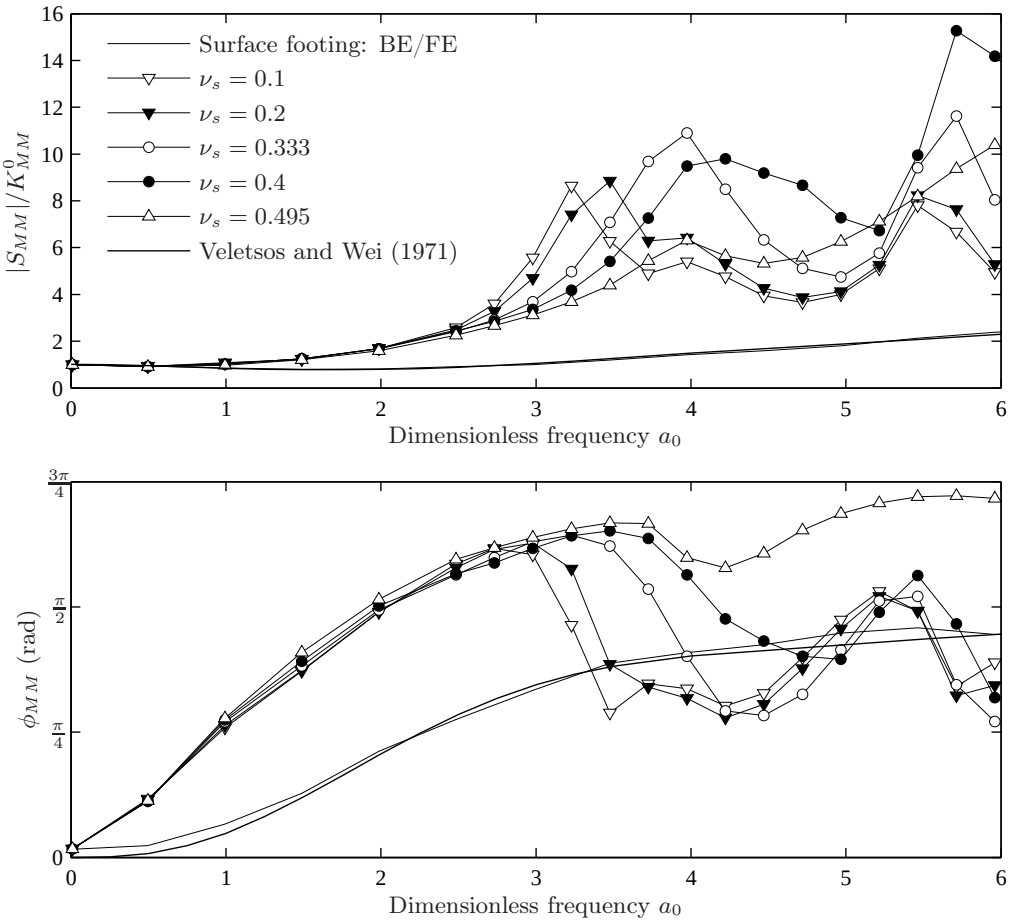

Figure 1.6: Rocking impedance: variation of Poisson's ratio. $G_s = 1.0$ MPa and $\eta_s = 5\%$.

$a_0 = 3.2$, whereas the first peak for $\nu_s = 0.4$ is placed close to $a_0 = 4.5$. However, the second local extremum is found at the frequency $a_0 = 5.5 - 5.7$ for all values of Poisson's ratio. This behaviour is explained by the fact that sliding and rocking impedances are governed by both shear wave propagation and compression wave propagation. More specifically, the first peak in the response corresponds to antiresonance of P-waves inside the caisson, whereas the second peak corresponds to antiresonance of S-waves. The latter is independent of the Poisson's ratio whereas an increase in ν_s involves an increase in c_P. Hence, the first peak in Figures 1.5–1.7 occurs at lower frequencies for lower Poisson's ratios.

The coupling impedance in Figure 1.7 follows the pattern of the horizontal and moment impedances. Hence, an increase in the frequency provides an increase in the magnitude of the coupling impedance over the normalized frequency range $a_0 \in]0;6]$. It is noted that the phase angle of the coupling impedance is close to π radians for $a_0 = 0$

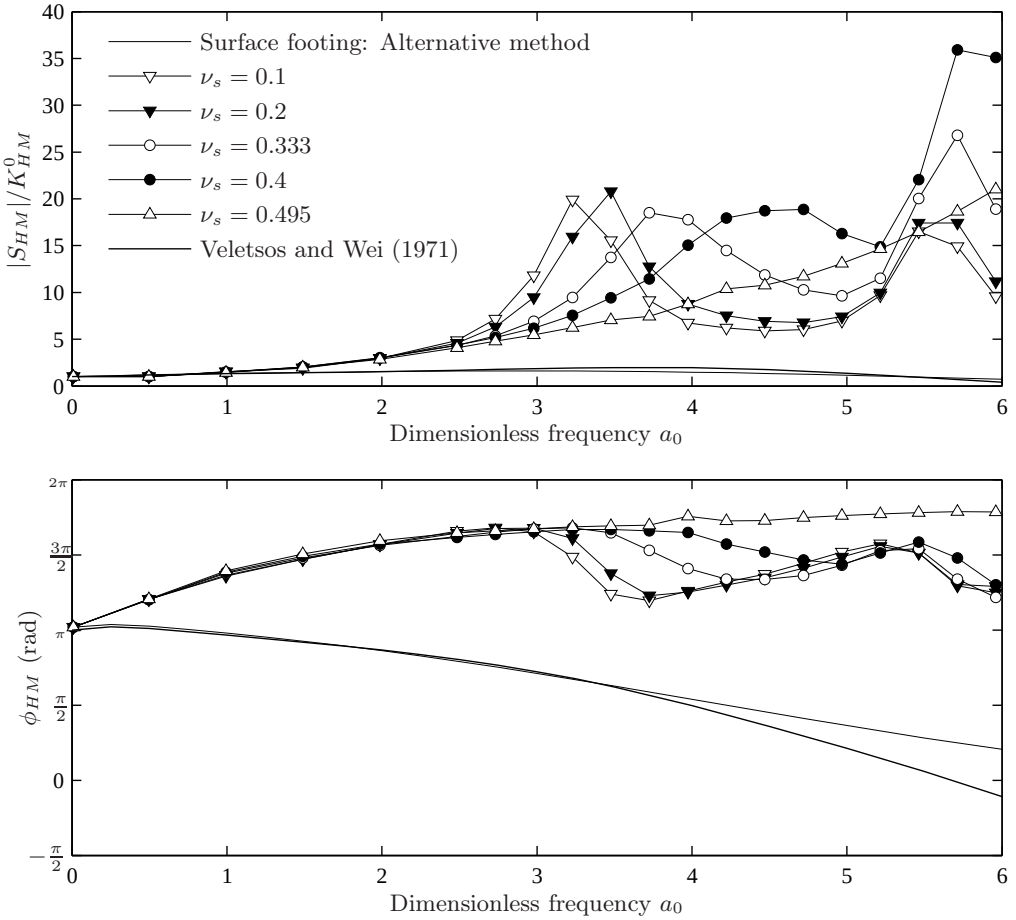

Figure 1.7: Coupling impedance: variation of Poisson's ratio. $G_s = 1.0$ MPa and $\eta_s = 5\%$.

and slightly increasing with the frequency in the range $a_0 \in]0;6]$. Accordingly the static stiffness components K^0_{HM} and K^0_{MH} are negative, see Table 1.2. It is generally observed that the coupling impedances of the suction caisson and the surface footing behave differently. Thus, in the case of the surface footing a decrease of both the magnitude and the phase of the coupling impedance with frequency is recorded in the interval $a_0 \in]0;6]$.

A few remarks on the impedance of the surface footing: The sliding and rocking impedance determined by the BE/FE model agrees very well with the analytical solution reported by Veletsos and Wei (1971). Furthermore, the coupling terms obtained by the alternative method (Andersen and Clausen 2005) is consistent with the coupling reported by Veletsos and Wei (1971). Note that the analytical solution with respect to the coupling term is an approximation, due to fact that the boundary conditions in the interface between the soil and the footing are partly relaxed. Finally, it is emphasized that the problem of determining the coupling between horizontal sliding and rocking

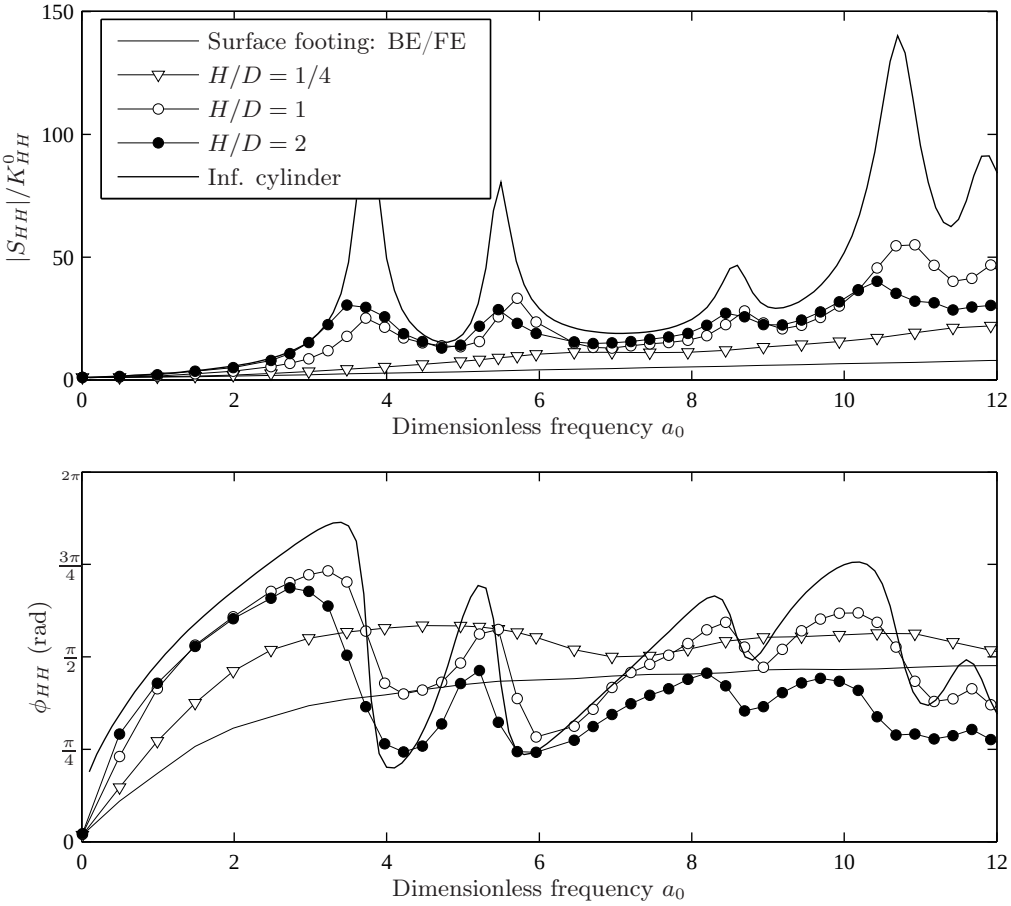

Figure 1.8: Sliding impedance: variation of skirt length. $G_s = 1.0$ MPa, $\nu_s = 1/3$ and $\eta_s = 5\%$.

only is encountered for the surface footing. The coupling between horizontal sliding and rocking for the suction caisson is described satisfactorily by the BE/FE model.

1.5.4 Dynamic stiffness—variation of skirt length

The variation of the coupled dynamic stiffness components with respect to a change in the skirt length H is presented in the following. The model properties are $G_s = 1$ MPa, $\nu_s = 1/3$, $\rho_s = 1000$ kg/m^3, $\eta_s = 5\%$, $E_f = 210$ GPa, $\nu_f = 0.25$, $\eta_f = 2\%$ and $t = 50$ mm. Again, $\rho_f = 0$ for the lid of the caisson and $\rho_f = \rho_s$ for the skirt in order to model a massless foundation. The magnitudes and the phase angles of the impedance for $H/D = 1/4$, 1 and 2 are shown in Figures 1.8–1.10 for the frequency range $a_0 \in]0;12]$. The magnitudes are normalized with respect to the static stiffness coefficients listed in Table **??**, and the results achieved with two numerical models of a massless surface footing

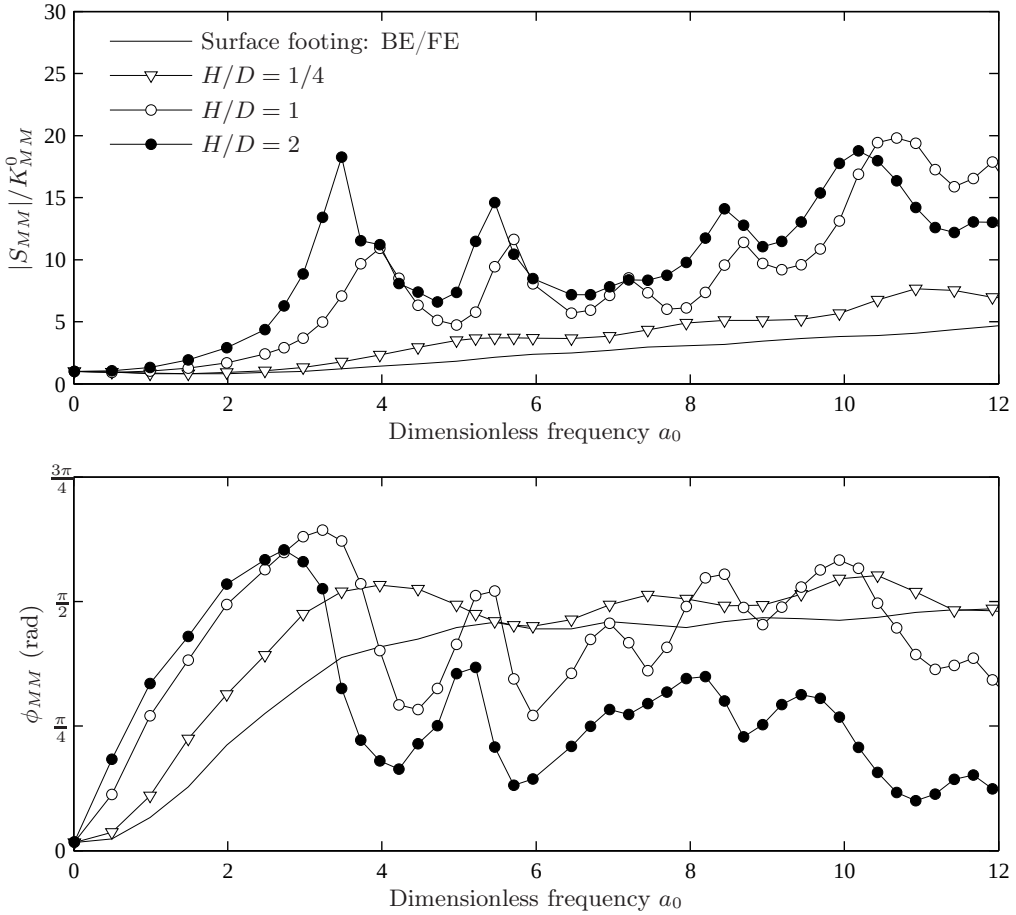

Figure 1.9: Rocking impedance: variation of skirt length. $G_s = 1.0$ MPa, $\nu_s = 1/3$ and $\eta_s = 5\%$.

are included for comparison, see Subsection 1.5.3. In addition to this, the horizontal sliding impedance of an infinitely long hollow cylinder ($H/D = \infty$) has been computed by application of the two dimensional BE/FE code TEA as described in Subsection 1.4.3 for the case of torsional vibrations. Evidently, a similar two-dimensional analysis cannot be performed for the rocking and coupling impedances. With reference to Figure 1.8, there is no indication of antiresonance of the waves inside the caisson with a relatively small embedment depth ($H/D = 1/4$), i.e. there are no local peaks in the normalized magnitude of the impedance component for sliding. Thus the dynamic behaviour is similar to that of the surface footing, though the increase of the impedance with increasing frequency is more pronounced for the skirted foundation than the surface footing. However, the sliding impedances for $H/D = 1$ and 2 are characterized by a number of local tips and dips. The peaks are not repeated with the normalized frequency interval $\Delta a_0 = \pi$. This is the case for the vertical and torsional impedances, where the location of the peaks

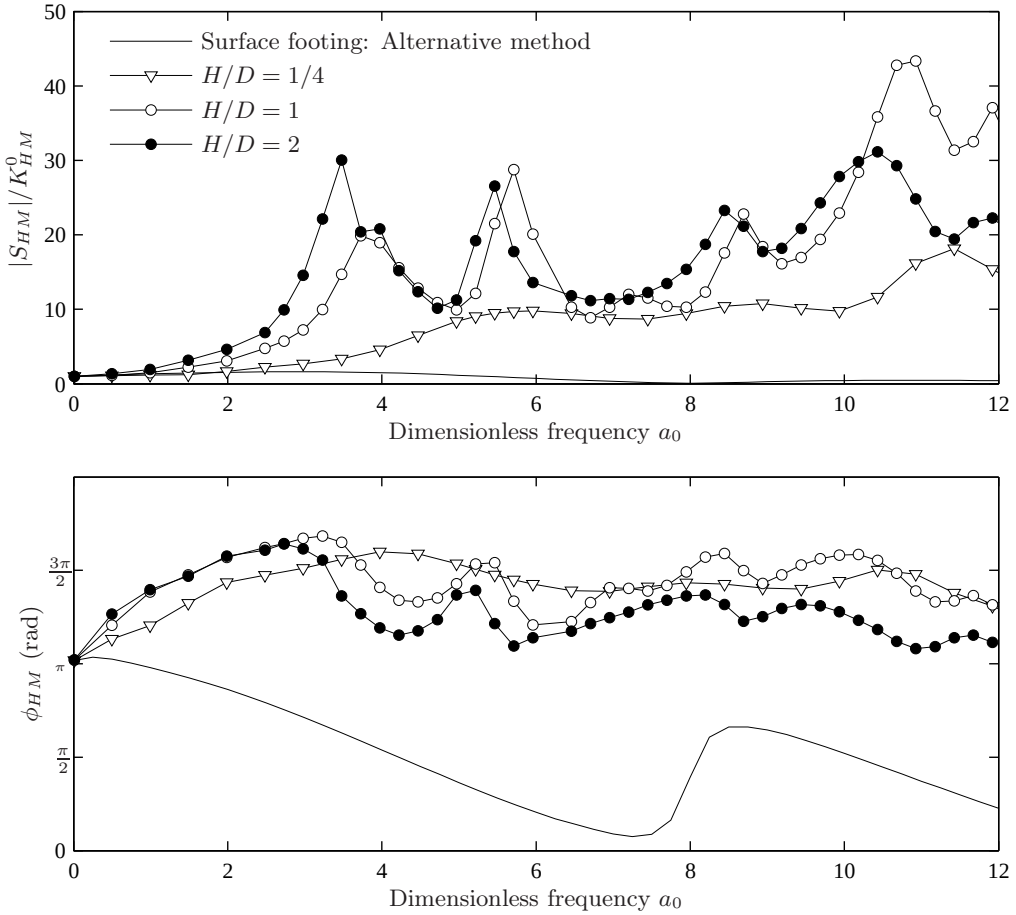

Figure 1.10: Coupling impedance: variation of skirt length. $G_s = 1.0$ MPa, $\nu_s = 1/3$ and $\eta_s = 5\%$.

are governed by the shear waves only. In contrast to this, the location of the peaks for the coupled sliding–rocking impedances are controlled by antiresonance of both shear waves and compression waves. Clearly, the locations of the peaks in the magnitude of the sliding impedance for $H/D = 1$ and 2 correspond to those for the infinitely long cylinder. Likewise, the variation of the phase angle ϕ_{HH} is similar for $H/D = 1$, 2 and ∞, cf. Figure 1.8. The magnitude of the horizontal impedance (Figure 1.8) seems to increase with skirt length. However, the change from $H/D = 1/4$ to $H/D = 1$ is significant, whereas only a small change is observed from $H/D = 1$ to $H/D = 2$. The magnitude of the impedance for $H/D = 2$ is actually below the impedance for $H/D = 1$ at high frequencies. This behaviour suggests that the horizontal vibrations are transmitted to the surrounding soil at relatively shallow depths. Hence, the effects of increasing the skirt length diminish with depth. This is not the case for the moment impedance in Figure 1.9, where the effects of increasing the skirt length enlarge with depth. These

tendencies are also evident in the static stiffness coefficients listed in Table 1.2. Finally, the coupling impedance in Figure 1.10 increases moderately with an increase of the skirt length, and again the phase angle is close to π radians for all frequencies. Otherwise, the overall response is similar to the horizontal and moment impedances.

1.5.5 High-frequency limit

In this subsection the high-frequency behaviour is formulated by limiting damping parameters (coefficients of a dashpot) with the intention of use in lumped-parameter models (Ibsen and Liingaard 2006b). The total geometrical damping is equal to the sum of the waves radiating from the skirts and the lid of the caisson. The limiting damping parameter for the horizontal vibration (C^{∞}_{HH}) consists of three contributions: shear waves radiating from the lid, shear waves radiating from the skirt parallel to the direction of loading, and compression waves radiating from the skirt perpendicular to the direction of loading. The high-frequency impedance for the rocking and coupling terms consist of similar contributions, see (Bu and Lin 1999; Gazetas and Dobry 1984; Gazetas and Tassoulas 1987; Fotopoulou et al. 1989; Wolf and Paronesso 1992) for further details. Assuming that both the lid and the skirts of the suction caisson are rigid, the limiting damping parameters C^{∞}_{HH}, C^{∞}_{MM} and C^{∞}_{HM} of the suction caisson are given by

$$C^{\infty}_{HH} = \rho_s c_S \pi R^2 + 2\rho c_S \pi RH + 2\rho c_P \pi RH, \tag{1.6a}$$

$$C^{\infty}_{MM} = \rho_s c_P \frac{\pi}{4} R^4 + 2\rho_s c_P \frac{1}{3} \pi RH^3 + 2\rho_s c_S \frac{1}{3} \pi RH^3 + 2\rho_s c_S \pi R^3 H, \tag{1.6b}$$

$$C^{\infty}_{HM} = -2\rho_s c_S \frac{1}{2} \pi RH^2 - 2\rho_s c_P \frac{1}{2} \pi RH^2 = C^{\infty}_{MH}. \tag{1.6c}$$

Note that waves radiate from both inside and outside the skirts, hence the factor '2' in front of the appropriate contributions in Equations 1.6a–1.6c.

1.6 Conclusion

The impedance of suction caissons with respect to torsional vibrations and coupled sliding–rocking vibrations has been analysed numerically, employing a three-dimensional coupled Boundary Element/Finite Element model in the frequency domain.

1.6.1 Torsional vibrations

The torsional dynamic stiffness has been analysed with respect to the variation of the stiffness due to a change in the skirt length H. The main conclusions are:

- The static torsional stiffness, K^0_{TT}, obtained with the BE/FE model has been compared with the results from a finite element analysis. There is good agreement between the estimations of K^0_{TT} provided by the two methods with a maximum deviation of 5.52%
- The magnitude of the static and dynamic torsional stiffness increases with skirt length.

- The torsional impedance of the suction caisson with a relatively small embedment depth ($H/D = 1/4$) varies smoothly with the frequency, whereas the torsional impedances for $H/D = 1$ and 2 are characterized by distinct peaks in the normalized magnitude close to $a_0 = 4$, 7 and 10.
- The oscillations are repeated for equal distances in frequency, corresponding to antiresonance modes in the soil inside the suction caisson.
- The torsional impedance of the suction caisson has been compared with the impedance of an infinite cylinder subjected to a torsional moment. The change with frequency in the magnitude and the phase angle of the impedance are equivalent for the suction caisson and the infinite cylinder.

1.6.2 Coupled sliding–rocking vibrations

The impedance of the coupled sliding–rocking vibrations have been analysed with respect to the effects of Poisson's ratio and the skirt length. The following conclusions can be made:

- The static stiffness has been calculated with a BE/FE model and a finite element model. The largest deviation of the results of the two models are 7.4%, 7.2% and 16.8% for the sliding, rocking and coupling terms, respectively.
- The two coupling terms between sliding and rocking are equal, i.e. $K^0_{HM} = K^0_{MH}$, within the accuracy of the analysis. The maximum deviation between K^0_{HM} and K^0_{MH} is 11%
- The sliding and rocking impedances are clearly dependent on the Poisson's ratio of the soil, and the local extremum in the magnitude of the impedance changes significantly with Poisson's ratio.
- The effects of increasing the skirt length diminish with depth with respect to the horizontal impedance. The effects of increasing the skirt length enlarge with depth with respect to the rocking impedance and the sliding–rocking coupling components.
- The coupled sliding–rocking impedances are characterized by a complex wave interference pattern in the soil inside the skirts. The local peaks in the magnitude of the impedance components are not repeated by $\Delta a_0 = \pi$, which is the case for the vertical and torsional impedance components. The location of the peaks for the coupled sliding–rocking impedances are controlled by antiresonance of both shear waves and compression waves.
- The analysis of the horizontal impedance for an infinite hollow cylinder clearly shows the anti-resonance frequencies of both shear waves and compression waves for the vibrating cylinder. The results agree very well with the horizontal impedance of the suction caissons.

Finally, it is noted that the high-frequency limits of the impedance components have been established for the skirted foundation. These will be applied in combination with the low-frequency impedances obtained with the BE/FE models in future formulations of lumped-parameter models of suction caissons.

Bibliography

Abaqus (2003). *ABAQUS—Version 6.4*. ABAQUS, Inc 2003, 1080 Main Street, Pawtucket, RI 02860-4847.

Andersen, L. and J. Clausen (2005). Impedance of surface footings on layered ground. *Submitted to Computers & Structures*.

Andersen, L. and C. Jones (2001). BEASTS — A Computer Program for Boundary Element Analysis of Soil and Three-dimensional Structures. ISVR Technical Memorandum 868, Institute of Sound and Vibration Research, University of Southampton.

Avilés, J. and L. E. Pérez-Rocha (1996). A simplified procedure for torsional impedance functions of embedded foundations in a soil layer. *Computers and Geotechnics 19*(2), 97–115.

Bu, S. and C. H. Lin (1999). Coupled horizontal-rocking impedance functions for embedded square foundations at high frequency factors. *Journal of Earthquake Engineering 3*(4), 561–587.

Emperador, J. M. and J. Domínguez (1989). Dynamic response of axisymmetric embedded foundations. *Earthquake Engineering and Structural Dynamics 18*, 1105–1117.

Fotopoulou, M., P. Kotsanopoulos, G. Gazetas, and J. L. Tassoulas (1989). Rocking damping of arbitrarily shaped embedded foundations. *Journal of Geotechnical Engineering, ASCE 115*, 473–490.

Gazetas, G. and R. Dobry (1984). Simple radiation damping model for piles and footings. *J. Engng. Mech. Div., ASCE 110*(6), 931–956.

Gazetas, G. and J. L. Tassoulas (1987). Horizontal damping of arbitrarily shaped embedded foundations. *Journal of Geotechnical Engineering, ASCE 113*, 458–575.

Houlsby, G. T., L. B. Ibsen, and B. W. Byrne (2005). Suction caissons for wind turbines. In *Proceedings of International Symposium on Frontiers in Offshore Geotechnics: ISFOG 2005*, Perth, Australia. Taylor & Francis Group, London.

Ibsen, L. B. and M. Liingaard (2006a). Dynamic stiffness of suction caissons—vertical vibrations. DCE Technical report 7, Department of Civil Enigineering, Aalborg University.

Ibsen, L. B. and M. Liingaard (2006b). Lumped-parameter models. DCE Technical report 11, Department of Civil Enigineering, Aalborg University.

Jones, C., D. Thompson, and M. Petyt (1999). TEA — a suite of computer programs for elastodynamic analysis using coupled boundary elements and finite elements. ISVR Technical Memorandum 840, Institute of Sound and Vibration Research, University of Southampton.

Luco, J. E. and R. A. Westmann (1971). Dynamic response of circular footings. *J. Engng. Mech. Div., ASCE 97*(EM5), 1381–1395.

Mita, A. and J. E. Luco (1989). Impedance functions and input motions for embedded square foundations. *Journal of Geotechnical Engineering, ASCE 115*(4), 491–503.

Novak, M. and K. Sachs (1973). Torsional and coupled vibrations of embedded footings. *Earthquake Engineering and Structural Dynamics 2*, 11–33.

Veletsos, A. and Y. Wei (1971). Lateral and rocking vibration of footings. *J. Soil Mech. Found. Engrg. Div., ASCE 97*, 1227–1248.

Veletsos, A. S. and V. V. Damodaran Nair (1974). Torsional vibration of viscoelastic foundations. *J. of Geotech. Engng. Div., ASCE 100*, 225–246.

Wolf, J. P. and A. Paronesso (1992). Lumped-parameter model for a rigid cylindrical foundation in a soil layer on rigid rock. *Earthquake Engineering and Structural Dynamics 21*, 1021–1038.

Wong, H. L. and J. E. Luco (1985). Tables of impedance functions for square foundations on layered media. *Soil Dynamics and Earthquake Engineering 4*(2), 64–81.